J. COMBIN. MATH. COMBIN. COMPUT. 127b (2025) 3033--3049

Journal of Combinatorial Mathematics and Combinatorial Computing
www.combinatorialpress.com/jcmcc

Theoretical study of charge transport and luminescence efficiency enhancement in OLED devices based on differential equation modeling

Yiheng Pang[1,✉]

[1] *Mechatronic Engineering and Automation School of Shanghai University, Shanghai, 200444, China*

ABSTRACT

Organic light-emitting diodes (OLEDs), as a new generation display and lighting technology, are critical for charge transport and luminescence efficiency enhancement. The study determines the potential, electron and hole concentrations in OLED devices based on Poisson's equation and current continuity equation, and fits the charge transport process in the devices with the drift-diffusion model. The differential equations are solved by improved Euler's method and iterative solution method to simulate the operating state of the OLED device. In conjunction with experiments, the enhancement effects of the OLED devices optimized based on the differential equation model in terms of charge transport and luminescence efficiency are analyzed. The optimized device and the comparison device exhibit the same partial pressure and a largely overlapping luminescence curve at 450~460 nm, but the optimized device lifetime and brightness are better than the comparison device. The charge transfer efficiency of the optimized device exceeded 99.99%, while that of the comparison device was lower than 95%. In addition, the light extraction efficiency of the optimized device is more than 20% higher than that of the comparison device, and it has the highest current efficiency, i.e., the optimized device has a better luminescence efficiency. The differential equation model is used in OLED devices to describe the processes of charge transport, optical properties, etc. The model can be used to systematically optimize the material properties and improve the overall efficiency of OLED devices.

Keywords: Differential equation modeling, Drift-diffusion model, Luminescence efficiency, OLED device

1. Introduction

Organic electroluminescent device (OLED) is a light-emitting diode composed of organic materials, and its device structure and light-emitting mechanism are interrelated, which together form the basis

✉ Corresponding author.
E-mail address: 13398638177@163.com (Y. Pang).
Received 10 January 2024; Revised 25 May 2024; Accepted 20 October 2024; Published Online 16 April 2025.
DOI: 10.61091/jcmcc127b-170

of OLED technology [1]. OLED development to the present time, also only has more than thirty years of development history, but OLED is now widely used, such as smart phones [2], high-end TV [3], tablet PCs [4], automotive display devices [5], smart lighting [6], photomedicine [7], wearable devices [8], functional textiles [9], etc., and its various performances can fully challenge the level of inorganic semiconductors, and in many aspects have reached the commercialization requirements [10]. Since C.W. TANG et al. reported low-voltage, high-efficiency organic small-molecule electroluminescent devices in 1987, OLED technology has gained rapid development after the commercial globalization of the production of OLED products in 1997, as well as used in automobile stereos, and is very promising to become the dominant technology for the next generation of displays [11-13].

At present, various R&D organizations around the world have invested a lot of manpower and resources in researching the basic theory of OLEDs, and some new characteristics of OLED devices have been discovered. However, in some aspects, organic semiconductors are still in a less perfect stage of development, and there are still many shortcomings and deficiencies that need to be addressed. For example, when the transient scanning voltage is applied to the OLED device, phenomena such as zero-current-voltage shift can be observed from its voltage-current curve, as well as the effect of performance stability under charge transfer, so it is necessary to further develop organic semiconductors to improve the performance and efficiency of organic electronic devices [14-17]. In addition, OLED devices are composed of several layers such as light-emitting layer, current-transporting layer and anode and cathode, and their structures mainly include the bottom and top structures, and the charge-transporting layer in the bottom structure is usually located between the organic light-emitting layer and the charge-injection layer, which is used to enhance the carrier transport and equalize the charge [18-19]. When an appropriate voltage is applied in an OLED device, the cathode injects electrons from the cathode end and the anode injects holes from the anode end, and the electrons and holes accumulate in the charge transport layer and are further injected into the emission layer. In the emissive layer, the electrons and holes meet, undergo a complex reaction and release energy which is emitted in the form of photons to form visible light [20-22]. Red light is emitted when a positive voltage is applied to the cathode (top of the emissive layer) and blue and green light is emitted when a positive voltage is applied to the anode (bottom of the emissive layer) [23]. By controlling the polarity and magnitude of the voltage, the color display of the OLED display can be achieved. And the molecular structure of the organic light-emitting materials in the emissive layer determines the color of the light and the luminescence efficiency [24-25]. In order to perfect the performance of OLED devices, their charge transfer and luminescence efficiency have to be optimized.

In this paper, a set of differential equation mathematical models is constructed to describe the charge transport, compounding, and luminescence processes in OLED devices, and the effects of key factors on device efficiency are explored. The spatio-temporal distribution of charges and excitons in the device is quantitatively described by establishing the drift-diffusion equation. The accuracy, truncation error, and stability problems in the solution process of the differential equations are also analyzed. The alternating solution method is adopted to solve the system of differential equations and the system of algebraic equations in charge transport in a joint manner, and the corresponding state vectors are derived for the time series. The study prepares flexible OLED devices based on the differential equation optimization model and compares them with conventional OLED devices to demonstrate the impact of the differential equation model on the performance enhancement of OLED devices.

2. Organic light-emitting diodes (OLEDs)

2.1. OLED structure

OLEDs [26] are mainly used in industries such as displays, lighting panels, wearables, and medical care. OLEDs are a sandwich-like structure, and a typical OLED device structure is shown in Fig. 1, with a single-layer structure in Fig. 1(a) and a multilayer structure in Fig. 1(b). The most basic OLED structure consists of three layers of anode, light-emitting layer, and cathode stacked in sequence, and this structure will lead to unbalanced carrier transport due to the mismatch of carrier transport capabilities of materials, thus obtaining a lower device efficiency. In order to balance the carrier transport, a multilayer OLED structure as in Fig. 1(b) was developed. The multilayer OLED structure generally consists of a stack of anode, hole injection layer (HIL), hole transport layer (HTL), light-emitting layer (LED), electron transport layer (ETL), electron injection layer (EIL), and cathode. The HIL and the EIL help to inject holes and electrons into the organic layer, which improves the carrier concentration and reduces the device turn-on voltage. The HTL and the ETL are inserted into the interface between the EML/HIL or the HTL and ETL are inserted between the interfaces of EML/HIL or EML/EIL, respectively, which help to transport holes and electrons to the EML for carrier complexation, thus increasing the carrier concentration inside the device or blocking carrier leakage to the electrodes and improving the device performance.

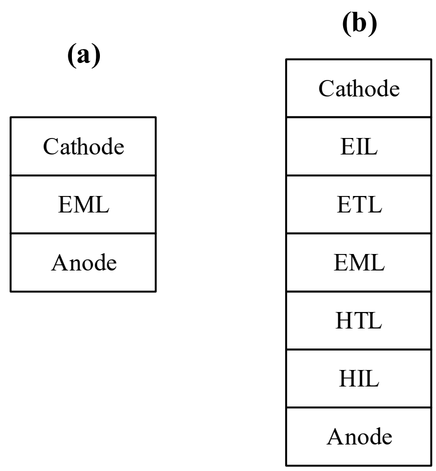

Fig. 1. Schematic diagram of typical OLED device structure

2.2. Illumination process

OLEDs are two-carrier-injected light-emitting devices that convert input electrical energy into light energy output. Figure 2 shows the light-emitting process of OLED.

1) Carrier injection: Under the action of an applied electric field, holes at the anode and electrons at the cathode are injected into the organic layer. In the injection process, the hole from the anode of the Fermi energy level jump to the adjacent organic material layer of the highest occupied molecular orbital (HOMO), the electron from the cathode of the Fermi energy level jump to the adjacent organic material layer of the lowest unoccupied molecular orbital (LUMO).

2) Carrier transport: in the applied electric field and the carrier between the Coulomb gravitational force, holes and electrons continue to the light-emitting region of the direction of the leap process.

3) Carrier composite: when the hole and electron transport to the light-emitting region, the two in the Coulomb gravitational force under the action of internal composite formation of excitons.

4) Radiative Leap: When an exciton returns to the ground state by radiative leap from the excited state, the device will emit fluorescence or phosphorescence. A single heavy state exciton can jump directly from the excited state to the ground state to emit fluorescence.

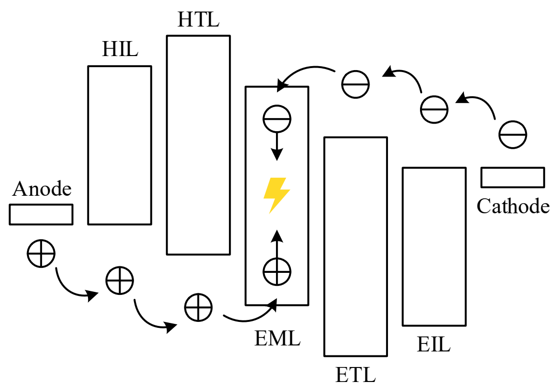

Fig. 2. Basic principle of OLED luminescence

2.3. OLED Preparation Process

The preparation process of OLED has more methods, which are mainly divided into the following two types of methods: vacuum vapor deposition and solution method. And the solution method can be divided into spin coating, inkjet printing, scraping, brushing, dipping and spraying.

The main method for commercial production of OLED full-colorized displays is the vacuum evaporation method. Vacuum vapor deposition refers to the method of heating the coating material in a vacuum environment to vaporize it into gaseous particles with a certain amount of energy, and the gaseous particles will be deposited onto the surface of the substrate to condense into a film. As a more cost-effective alternative, the solution method for OLEDs has been proposed. Compared to vacuum vapor deposition, the solution method is simpler to operate and has a higher material utilization rate.

Solution method refers to the method of dispersing materials in a well-dispersed solvent to form a homogeneous solution, and then depositing the materials on the substrate by spin-coating, printing, squeegee-coating, or spraying, etc. The solution method is also used for the preparation of OLEDs. The solution method of OLED preparation is mainly categorized into spin-coating, scraping, spraying and inkjet printing.

1) Spin-coating method means that after dropping the solution on the substrate, the spin-coater is activated, and the substrate is rotated at high speed under the set spin-coating speed and duration, and finally annealed to remove the solvent to form a film in a certain way.

2) Scraping is a method of placing the ink material on the substrate, moving the scraper to evenly scrape the ink material onto the surface of the substrate, and then annealing to remove the solvent film.

3) Spraying is a process in which a solution is uniformly sprayed onto the surface of an object by means of a spray gun. In the spraying process, the solution passes through the nozzle of the spray gun and is sprayed on the substrate in a high-speed jet to form a film.

3. Differential equation modeling of charge transport and luminous efficiency of OLED devices

3.1. Numerical models

3.1.1. Drift-diffusion model. Describing the charge transport phenomena inside OLED devices through Poisson's equation [27] and the continuum equation for electron and hole currents are complex methods. The Poisson equation describes the relationship between electrostatic potential and charge. However the distribution of electrons and holes in the device is not known in advance. In this case the Poisson equation is applied in combination with the electron and hole current continuity equations to determine the electrostatic potential, and the own concentrations of electrons and holes. A set of equations for the drift-diffusion model [28] for device simulation is given in the steady state:

$$\Delta\phi = \frac{q}{\varepsilon_s}(n - p - D) \tag{1}$$

$$\frac{1}{q}\nabla.J_n = R(n, p) \tag{2}$$

$$\frac{1}{q}\nabla.J_p = -R(n, p) \tag{3}$$

where: ϕ is the electrostatic potential.

n and p are the densities of electrons and holes, respectively.

The electric field E is defined as $E = -\nabla\phi$.

q is the unit charge.

ε_s is the dielectric constant of the semiconductor.

$D(x, y) = N_D^+(x, y) - N_A^-(x, y)$ is the net doping concentration. R is the net binding ratio. R is assumed to be the Shockley-Read-Hall binding process:

$$R(n, p) = \frac{(np - n_i^2)}{t_p(n + n_i) + t_n(p + n_i)} \tag{4}$$

where t_n and t_p are the electron and hole lifetimes, respectively. Their masses are determined experimentally. Using a similar solution method, other carrier production and binding models can also be included. The collisional ionization and photon lepton carrier current densities J_n and J_p are given in the following equations:

$$J_n = -q\mu_n n\nabla\phi + qD_n\nabla n \tag{5}$$

$$J_p = -q\mu_p n\nabla\phi + qD_p\nabla n \tag{6}$$

where the carrier mobility μ_n and μ_p are determined by the carrier density and the electric field. The diffusion coefficients D_n and D_p are assumed to satisfy the Einstein relation:

$$\begin{aligned} D_n &= V_T\mu_n \\ D_p &= V_T\mu_p \end{aligned} \tag{7}$$

where the thermal voltage is defined as $V_T = K_B T_{L/q}$, T_L is the lattice temperature, and K_B is the Boltzmann constant, and q is the unit charge.

3.1.2. Boundary conditions. The Poisson equation for the drift-diffusion model is an elliptic equation. The problem of determining the solution of such equations is a margin problem. In a one- or two-dimensional simulation, it is to solve an unknown function that satisfies both the equations and the margin constraints in a certain interval or region. Mathematically, there are two types of boundary conditions or edge-value constraints to be satisfied by the function to be solved:

1) Type I boundary conditions, also known as Dirichlet conditions, which give the value of the function to be found on the boundary.

2) Type II boundary conditions, also known as Neuman conditions, which require that the normal gradient of the to-be-function at the boundary be a given value.

3.2. Numerical solution of differential equations

3.2.1. Basic Model. The analysis of charge transport in OLED devices requires solving a system of differential equations and a system of algebraic equations jointly. By solving a system of differential equations, we mean to find the numerical solution of the differential equations, i.e., to find the corresponding system state vector $y_0, y_1, y_2, \cdots, y_n$ step by step for the time series $t_0, t_1, t_2, ..., t_n$, under certain initial value conditions.

If for the differential equations:

$$\frac{dy}{dt} = f(y,t) \tag{8}$$

Let the initial value be $y(t=t_0) = y(t_0)$. If the calculation step is taken to be $h = t_n - t_{n-1} (n = 1, 2, \cdots)$, the exact value $y(t_1)$ of y at the moment t_1 should be:

$$y(t_1) = y(t_0) + \int_0^1 f(y,t)dt \tag{9}$$

In practice, the integral term is approximated, resulting in different numerical solutions.

When taking $y_i \approx y_0 + f(y_0, t_0)h$, that is, the derivative of $y(t)$ is considered to be constant in the interval $[y_0, y_i]$, that is, the approximation takes $y(t)$ as a straight line with a slope of $y_0^{'}$, that is, the derivative of the beginning of the interval. This method of numerical solution of differential equations is called Euler's method.

Some important properties of the numerical solution method are discussed below in order to select the numerical solution of the differential equation applicable to the charge transport process of the OLED device and to pay attention to the problems that may arise in the solution.

3.2.2. Higher- and lower-order algorithms, accuracy and truncation error. For Equation $\frac{d}{y}dt = f(y,t)$, the Taylor series expansion formula shows that in the $t_n \sim t_n + 1$ time zone there is:

$$y_{n+1} = y_n + y_n^{'}h + \frac{y_n^{''}}{2!}h^2 + \cdots + \frac{y_n^{(m)}}{m!}h^m + \cdots \tag{10}$$

When the first-order derivative term of the above equation is taken to approximate the computation of y_{n+1}, i.e., set $y_{n+1} \approx y_n + y_n^{'}h$, the numerical integration result is said to have first-order accuracy, and the truncation error, i.e., the deviation of the true value from the approximated computed value, can be known from the nature of Taylor poles as:

$$\frac{y^{n}(\xi)}{2!}h^2 = o(h^2) \quad \xi \in [t_n, t_{n+1}] \tag{11}$$

Called the second-order truncation error, which is Euler's method. Theoretically analyzed: general k-order accuracy and numerical calculation formula with $(k+1)$-order truncation error. Improved Euler method has second-order accuracy and third-order truncation error. Its accuracy is higher than Euler's method. Implicit integral method has second order accuracy, third order truncation error i.e. its accuracy is comparable to the improved Eulerian method. When the value of k is high, i.e., when higher order derivatives are taken for Taylor poles for approximation, the corresponding algorithm is called higher order algorithm and vice versa, it is called lower order algorithm.

3.2.3. Numerical stability issues. A very important issue in the numerical solution of differential equations is the tendency of the error formed in the previous step of the computational process to change in the subsequent time-steps of the computation: whether it is convergent or divergent, i.e., the stability problem. The problem of numerical stability is closely related to the characteristics of the physical problem itself, as well as to the computational method and the computational step size used. Theoretical analysis shows that the domain of numerical stability of implicit computational methods is much larger than that of explicit ones. When the explicit integration method is used, the choice of the step size is limited by the minimum time constant in the differential equation, which otherwise leads to incorrect calculation results.

3.3. Methods for solving differential and algebraic systems of equations

When applying the numerical solution method to calculate the charge transport process of an OLED device, both the differential equation and the set of algebraic equations must be solved within each integration step. For this purpose, there are two different methods: the alternating solution method and the associative solution method. This section focuses on the alternating solution method.

The differential equation and the system of algebraic equations describing the charge transport process can be written in general form as:

$$\begin{cases} px = f(x, y) \\ g(x, y) = 0 \end{cases} \tag{12}$$

When the numerical solution of a differential equation is by explicit integral method, the principle and procedure of the alternating solution method is relatively simple. Taking the explicit Euler method as an example, for the integration step from moment t to $t+\Delta t$, $x(t)$ and $y(t)$ at moment t are known quantities such that the computational steps are:

1) Apply Euler's formula to the differential equation to calculate the state vector $x(t+\Delta t)$, i.e.:

$$x(t+\Delta t) = x(t) + \Delta t f[x(t), y(t)] \tag{13}$$

2) Apply $x(t+\Delta t)$ to solve the algebraic equation, i.e., solve it:

$$g[x(t+\Delta t), y(t+\Delta t)] = 0 \tag{14}$$

This yields $y(t+\Delta t)$.

This yields $x(t+\Delta t)$ and $y(t+\Delta t)$ at moment $t+\Delta t$, which will be used in the calculation of the next integration step. The above steps are in principle applicable to all explicit integration methods. Since the final results $x(t+\Delta t)$ and $y(t+\Delta t)$ do not satisfy the algebraic and differential equations at the same time, this results in a certain error, called the handover error.

3.4. Analytical process based on improved Euler's method and iterative solution method

In charge transport analysis with low accuracy requirements and short simulation time, the dynamics of the prime mover and the speed control system are often ignored and the mechanical power is considered to be constant. This section discusses the charge transport and luminescence efficiency of OLED devices for solving the differential equations by the improved Euler method [29] and the network equations by the iterative solution method [30]. The flow framework for the dynamic analysis of OLED device charge transport based on the improved Eulerian method is shown in Fig. 3. The component model used in this section can be further simplified, if the convex pole effect is ignored and the classical second-order model with constant $E_q^{'}$ is used, and the load is adopted as a constant impedance model, solving the network equations can be conveniently carried out in the complex domain for solving a set of complex linear algebraic equations without having to make iterative calculations, and only the dynamics of the OLED device charge is considered in the analysis.

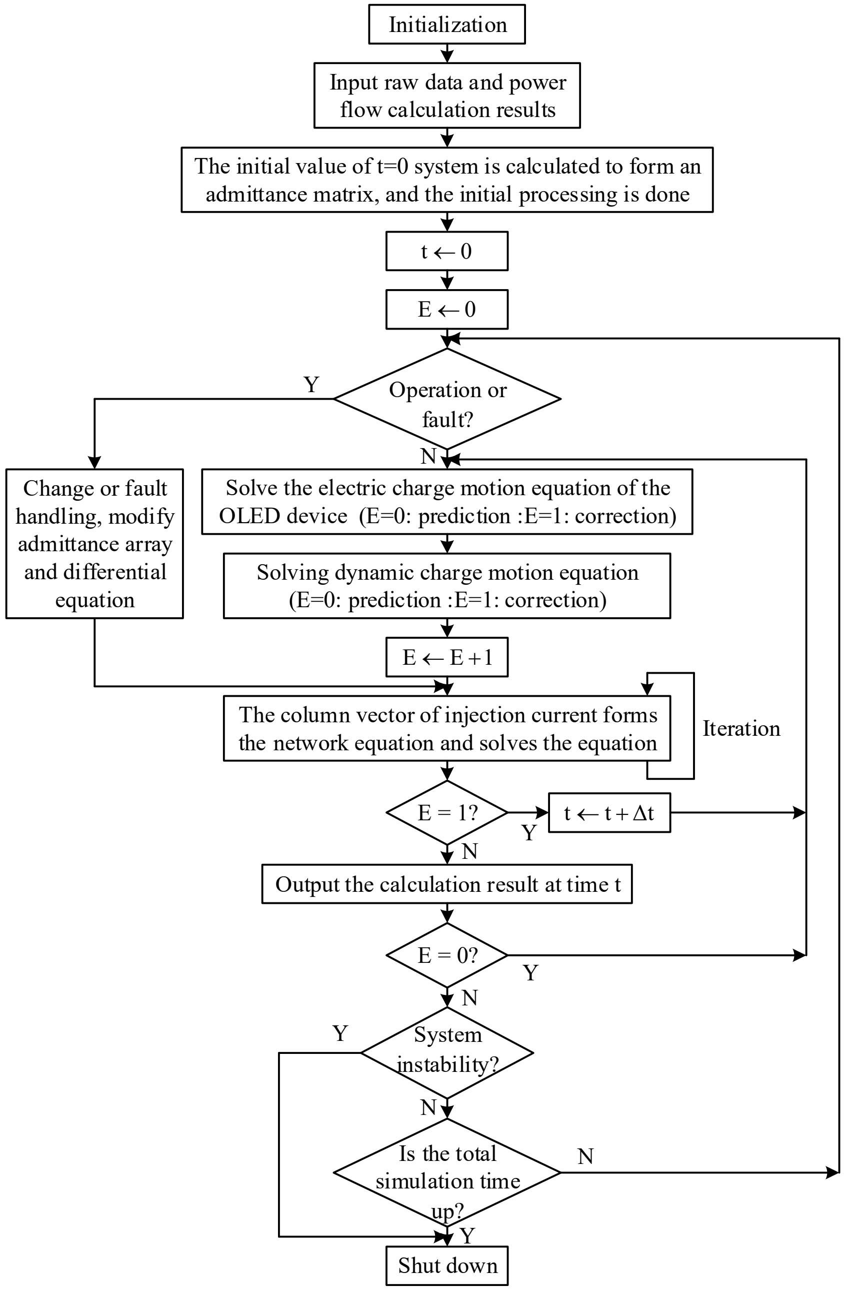

Fig. 3. The flow chart of the transient analysis of Euler method was improved

4. Study of rapid patterning methods for highly conductive PEDOT: PSS electrodes

In this section, the optimization of OLED device structure, material parameters and preparation process is based on the differential equation model considering the effects of electric field, charge diffusion and other factors. PEDOT: PSS is selected as the main material to prepare the flexible OLED device, and the performance of the device, such as efficiency, brightness and lifetime, is tested to verify the accuracy and reliability of the differential equation model.

4.1. Experimental materials

The materials used for the experiments in this paper include:

Polyethylene dioxythiophene: poly(styrenesulfonate) (PEDOT:PSS), specification parameter: PH 1000.

Polyethylene dioxythiophene: poly(styrenesulfonate) (PEDOT:PSS), specification parameter: AI 4083.

2,4-Hexadiyne-1,6-diol (Hexa-2,4-diyne-1,6-diol), Specification parameters: ≥98.0%.

Dimethyl sulfoxide (DMSO), Specification parameters: ≥99.9%.

1,3-di-9-carbazolylbenzene (m CP), Specification parameters: 99.9%.

Tris(2-phenylpyridine)iridium(Ir(ppy)3), Specification parameters: 99.9%.

1,3,5-Tris[(3-pyridinyl)-3-phenyl]benzene (TmPyPB), Specification parameters: 99.9%.

Chlorobenzene (CB), Specification parameters: ≥99.9%.

Lithium fluoride (LiF), Specification: 99.9%.

Aluminum (Al), Specification: 99.9%.

4.2. PEDOT: Patterning of PSS electrodes

1) Cleaning of glass bottles: Place the glass bottles in acetone for ultrasonic treatment for 10min, then place the glass bottles in anhydrous ethanol for ultrasonic treatment for 10min, take out the bottles and blow them dry with N2, and then place them in an oven at 120℃ for drying for 2h for spare.

2) Cleaning of flexible substrate: Polyethylene terephthalate (PET) substrate cut into 20mm × 20mm square pieces, placed in anhydrous ethanol ultrasonic treatment for 10min, remove the PET with N_2 blow-dry spare.

3) Configuration of modified PEDOT:PSS ink: Pipet 5 ml of PEDOT:PSS (Clevios PH1000) and filter it into a glass bottle using a 0.45 μm aqueous filter tip. Then measure 1mL of filtered PEDOT:PSS (Clevios PH1000) with a pipette gun, add it to the empty glass bottle, and repeat the measurement for 5 bottles. 0mg, 4mg, 6mg, 8mg, and 10mg of HDD crosslinkers were weighed respectively, mixed into the PEDOT:PSS ink measured before, stirred magnets were added, glass bottles were wrapped in tin foil to isolate light, and stirred at room temperature (20 °C) for 12h to prepare PEDOT:PSS:HDD mixed inks with concentrations of 0mg/mL, 4mg/mL, 6mg/mL, 8mg/mL, and 10mg/mL.

4) Patterning preparation of PEDOT:PSS electrodes: PET was treated with UVO for 30 min, and then the PET was placed on the vacuum suction cup of the spin-coater, and 80 μL of PEDOT:PSS:HDD ink was measured and dripped uniformly on the PET, and after the ink was spread out well, it was spin-coated at 1200 rpm for 90 s to make the PEDOT:PSS:HDD film. The metal template was placed on the PEDOT:PSS:HDD film and exposed with 254 nm UV light for 60 s. Then the PEDOT:PSS:HDD film was developed in deionized water for 60 s, and then annealed for 30 min at 120°C on a hot stage to obtain the patterned transparent electrode X-PEDOT:PSS.

4.3. Preparation flow of flexible OLEDs

After successfully preparing transparent patterned flexible X-PEDOT:PSS electrodes, green phosphorescent OLED devices were further prepared based on such electrodes. The hole transport layer PEDOT:PSS (AI4083) was filtered through a 0.45 μm aqueous filter head and dropped on the patterned X-PEDOT:PSS electrode, and after being spread evenly and spin-coated at 4000 rpm for 90 s, it was placed on a 120 ℃ hot stage and annealed for 15 min to complete the preparation. The light-emitting layer mCP:Ir(ppy)3 was mixed and vaporized in the ratio of 10:1. TmPyPB was vaporized at 0.2 nm/s, LiF at 0.004 nm/s. Al at 0.5 nm/s.

4.4. Characterization of film and device properties

After the electrode films were prepared, their properties were characterized using techniques such as four-probe, step meter, UV absorption spectrometer, and optical microscope. After preparation of the light emitting devices, their luminescent properties were characterized using a DC current source Keithley 2400 and a chromatic photometer PR 655. All the tests were carried out in an air environment without any encapsulation.

4.5. Optimization of device charge transport and luminescence efficiency enhancement effect

4.5.1. Analysis of photophysical properties of PEDOT:PSS molecules. In order to investigate the photophysical properties of the OLED devices designed based on the differential equation modeling in this paper, the UV-visible absorption spectrum (UV-Vis), photoluminescence spectrum (PL), and phosphorescence spectrum (Ph) of PEDOT:PSS molecules in toluene solution (10-5 M) were tested. The UV-Vis absorption and photoluminescence spectra were tested at room temperature, while the phosphorescence spectra were tested at a low temperature of 80K.

Figure 4 shows the UV-visible absorption spectrum, PL spectrum and phosphorescence spectrum of PEDOT:PSS molecule in toluene solution. From the absorption spectra, it can be seen that the PEDOT:PSS molecule has a broad absorption band between 350 nm and 400 nm, which belongs to the n-π* absorption and π-π* absorption of aromatic groups. In addition to this, the molecule PEDOT:PSS exhibits a higher intensity narrow absorption peak between 410 nm and 460 nm, which is located at 430 nm and belongs to the short-range charge transfer absorption due to multiple resonance effect. As seen from the PL spectra at room temperature, the molecule PEDOT:PSS exhibits azure emission and shows narrow band emission at 460 nm. At a low temperature of 80 K, the molecule PEDOT:PSS exhibits phosphorescence emission with a narrow half-peak width, reaching the highest intensity absorption peak at 527 nm. The structural relaxation and vibration of the molecule are frozen at low temperature, indicating that the structural relaxation and vibration of the molecule are suppressed by its own rigid structure.

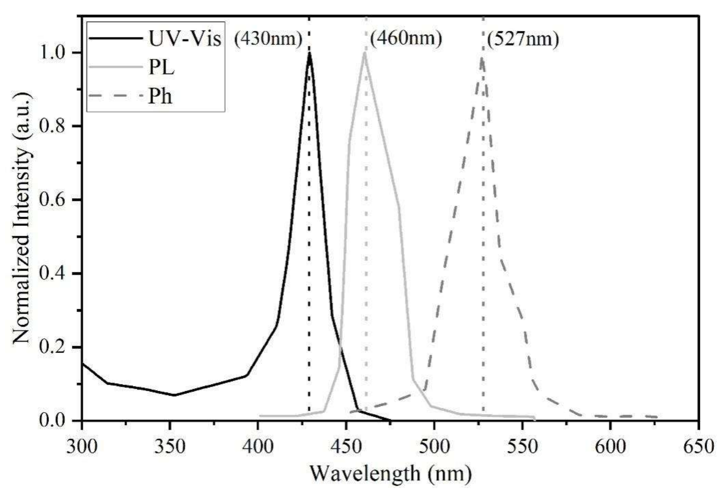

Fig. 4. The UV-vis absorption, PL and Ph spectra of molecules in toluene

To verify the thermally activated delayed fluorescence (TADF) properties of PEDOT:PSS molecules, Fig. 5 shows the PL spectra in toluene solution after nitrogen and oxygen bubbling treatment. The PL spectra of TADF materials are more sensitive to oxygen because oxygen molecules can burst trilinear excitons and have less effect on unilinear excitons. After the toluene solution containing PEDOT:PSS molecules was bubbled with oxygen, the fluorescence intensity of the PL spectra was significantly weakened, and this part of the fluorescence intensity decay corresponds to the trilinear excitons that should have been converted to unilinear excitons, which could not be efficiently utilized after they were burst by the oxygen molecules, which indirectly proves the existence of the process of the anticlonal interphase transitions of the trilinear excitons in the PEDOT:PSS molecules.

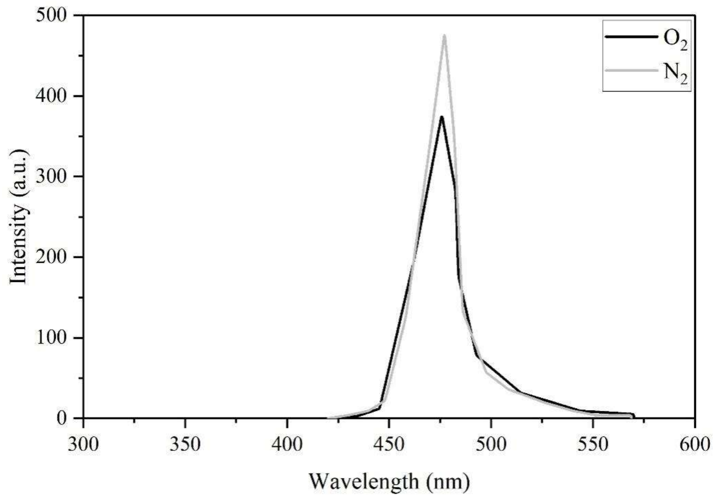

Fig. 5. The PL spectra of the molecules in nitrogen or oxygen

4.5.2. Optimizing Device Luminous Performance and Lifetime Evaluation. In order to investigate the effect of differential equation modeling on the stability of OLED devices with PEDOT:PSS molecules as the host material, device testing was performed using PEDOT:PSS solution. It was ensured that the devices were of the same type and thickness of the layer materials except for the main body material of the luminescent layer under study, and the thickness of the luminescent layer used was 100A. The differential equation model was optimized with Ir(ppy)3 dye for conventional OLED devices, while Alq_3 and CBP dyes were chosen to prepare two blue fluorescent contrast OLED devices, denoted as X1, X2, and X3, respectively, for performance comparison.

Figure 6 demonstrates the luminescence performance curves of the three devices. Fig. 6(a) shows the relationship between device voltage and current density, and it can be seen that all three curves exhibit an increase in voltage with increasing current, and both exhibit similar partial voltages at the same current intensity. Figure 6(b) shows the normalized spectra of the devices, and it can be seen that the emission peaks of the 3 devices are standard single peaks without other emission peaks, and the maximum luminescence wavelengths are between 450~460 nm, which are located in the blue light band. And the three devices show nearly overlapping emission curves. It can be assumed that the different dyes will not change the luminescent properties of the PEDOT:PSS molecule as the main material itself.

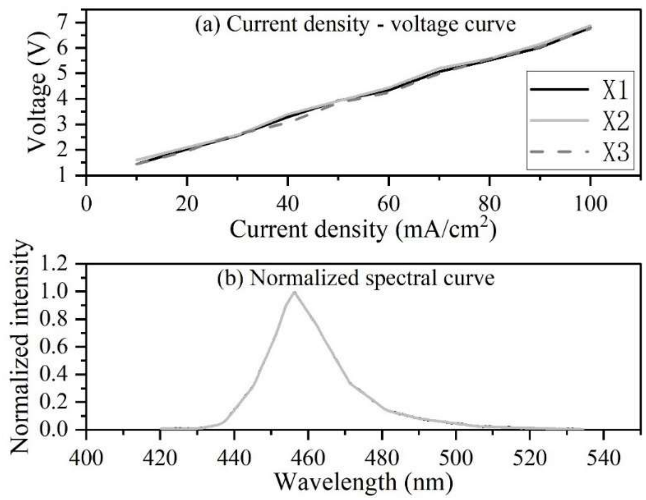

Fig. 6. The luminescent performance curve of the device

Figure 7 shows the lifetime-voltage curves for each device, and the device tests were performed at J = 40 mA/cm2. It can be found that the OLED devices with different dyes exhibit similar initial brightness among them, i.e., the initial brightness at time 0h is around 100%. The device brightness gradually decreases during operation, where X1 runs to 95h when it stops running, i.e., its lifetime is about 95h. As for the device voltage change, it can be seen that the device life after optimization through the differential equation model is higher and the voltage change before and after the degradation of the device is reduced to a certain extent. It can be considered that the differential equation model helps to optimize the design and operating conditions by describing the aging, thermal effects, and electrical characteristics of the OLED device, which prolongs the life of the device.

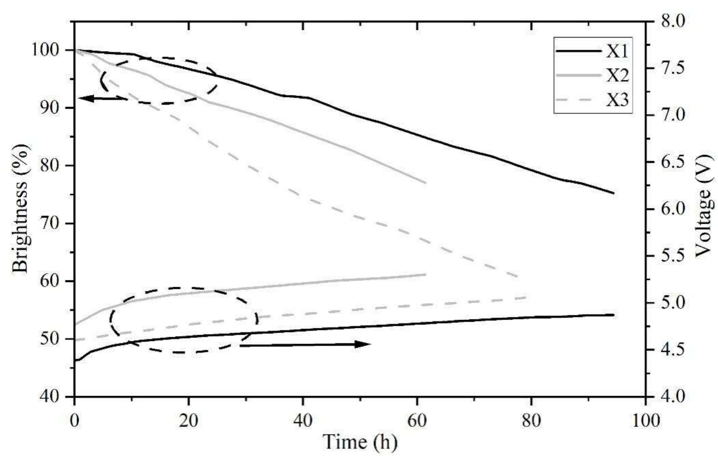

Fig. 7. Life-voltage curve for each device

4.5.3. Comparative analysis of charge transport efficiency. The charge transfer barrier can directly affect the performance parameters of the image sensor such as full trap capacity, charge transfer efficiency, etc. When the sensor is placed in a light environment, the process of photogenerated electrons accumulating in the OLED device from the beginning of the accumulation to the end of the accumulation is known as the exposure stage of the pixel. At the end of the exposure stage, the charge accumulated during the exposure of the OLED device is transferred to the OLED device node by applying a high voltage to the pixel transfer gate.

The charge transfer efficiency (CTE) is defined as a percentage of the ratio of the number of photogenerated electrons transferred to the OLED device node to the total number of electrons accumulated in the OLED device, and is expressed as follows:

$$CTE = \frac{N_t}{N_{col}} \times 100\% \tag{15}$$

where N_{col} is the total number of photogenerated electrons accumulated in the OLED device and N_t is the number of photogenerated electrons transmitted to the nodes of the OLED device.

The full well capacity (FWC) is defined as the maximum charge that can be accommodated in the OLED device in e^-. The equilibrium full-well (EFWC) under dark conditions has a value approximately equal to the number of electrons obtained by integrating the OLED device capacitance (C) between the clamp voltage (V_{pin}) and the voltage at which the equilibrium full-well capacity is reached during the exposure stage (V_{sat}), which is expressed as follows:

$$EFWC = \frac{1}{q}\int_{V_{pin}}^{V_{sat}} C(V)dV \tag{16}$$

When the clamp voltage of the OLED device is large and the potential of the channel transmission region is low, it is easy to generate a charge transport barrier, and the OLED device optimized by solving the differential equation model is subjected to an N-type ion injection at the interface with the transmission channel to adjust the potential distribution of the transmission channel and reduce the charge transport barrier.

The final obtained electron transport curves of each device are shown in Fig. 8. The data in the figure show that the EFWC of the X1 device is $7217e^-$, and before the start of the exposure stage, the transmission tube is turned on to reset the OLED device, and the number of electrons in the OLED device after reset is $5.59\times10^{-4}e^-$, and the electrons in the OLED device are transmitted to the node, and at this time, the OLED device is in a fully depleted state. At the end of the exposure stage, the number of electrons in the OLED device is $8639e^-$. In the transmission stage, the transmission tube is turned on, and the number of electrons within the OLED device after transmission is $6.5510^{-4}e^-$. According to the charge transfer efficiency calculation formula, the charge transfer efficiency of the OLED device optimized by the differential equation model reaches 99.99%, and the charge transfer efficiency of the X2 and X3 devices is calculated to be less than 95% by the same calculation.

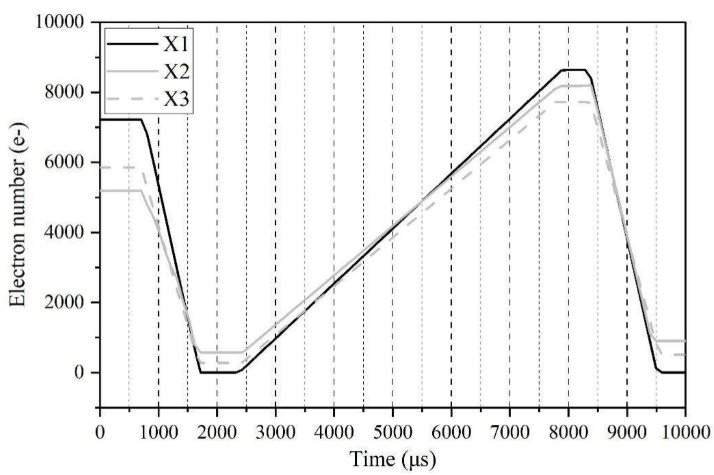

Fig. 8. Electronic transmission curve of OLED devices

4.5.4. Light Extraction Efficiency and Current Efficiency Measurement. The light extraction efficiency reflects the degree of optimization of the device structure for light extraction, and this section explores the performance effect of OLED devices optimized based on the differential equation model in terms of light extraction efficiency (LEE). Again, X2 and X3 devices are used as comparisons, and optical measurements are performed in a dark room to avoid external light interference. The light extraction efficiency of different devices under the condition of 20~400nm photonic crystal etching depth is measured to verify the stability of the light extraction efficiency of the optimized devices.The formula for calculating the LEE is as follows:

$$LEE = \frac{P_{zout}^{+}}{P_x^{+} + P_x^{-} + P_y^{+} + P_y^{-} + P_z^{+} + P_z^{-}} \times 100\% \tag{17}$$

P_{zout}^{+} is the light-out power of the light-out plane in air, and $P_x^{+} + P_x^{-} + P_y^{+} + P_y^{-} + P_z^{+} + P_z^{-}$ is the normal light-out power of the six faces of the closed hexahedron surrounding the point source, respectively, which can be calculated as the total light-out power of the source.

Fig. 9 shows the variation of light extraction efficiency with etching depth for the three devices. From the figure, it can be seen that the device optimized by the differential equation model (X1) has a significant improvement in the light extraction efficiency at different etching depths compared with the X2 and X3 devices. When the etching depth is 400mn, the X1 device shows the highest light extraction efficiency, which is 40.79% and 22.27% higher than the X2 and X3 devices, respectively. This has a certain guiding significance for the fabrication of high luminous efficiency using the differential equation model.

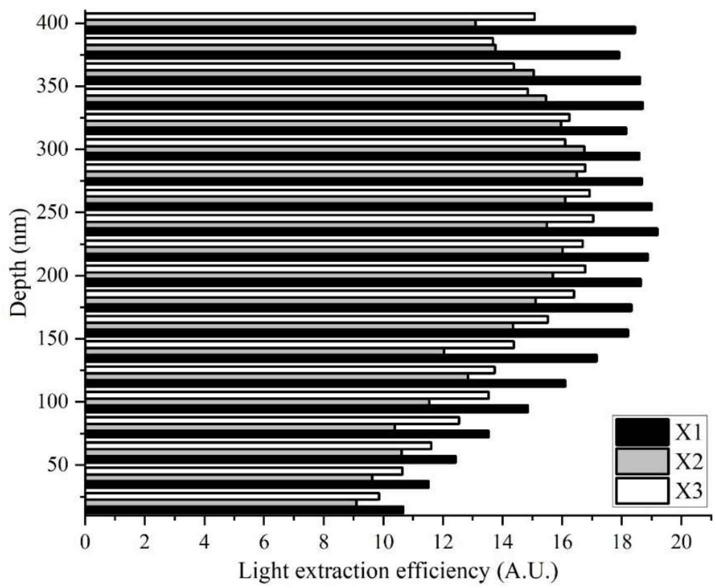

Fig. 9. The efficiency of the three devices is changed by the depth of the etch

This section measures the current efficiency at different current densities, reflecting the light-emitting intensity of the device under the unit current, side by side with the luminous efficiency of each device. Figure 10 shows the trend of luminescence efficiency of different devices with current efficiency. From the figure, it can be seen that the X1 device has the highest current efficiency of 3.57 cd/A. Since the luminescence efficiency of the device is not only related to carrier injection, but also related to the degree of balance between the injection of electrons and holes in the device. The OLED device material optimized by the differential equation model is more conducive to the injection of holes in the device, so the luminescence efficiency of the device is relatively high. It can also be seen from the figure that the current density of the X1 device is relatively large, thus it can be proved that the differential equation model improves the efficiency of hole injection in the device, and the chances of electron and hole compounding increase, so the luminescence efficiency of the device is also improved.

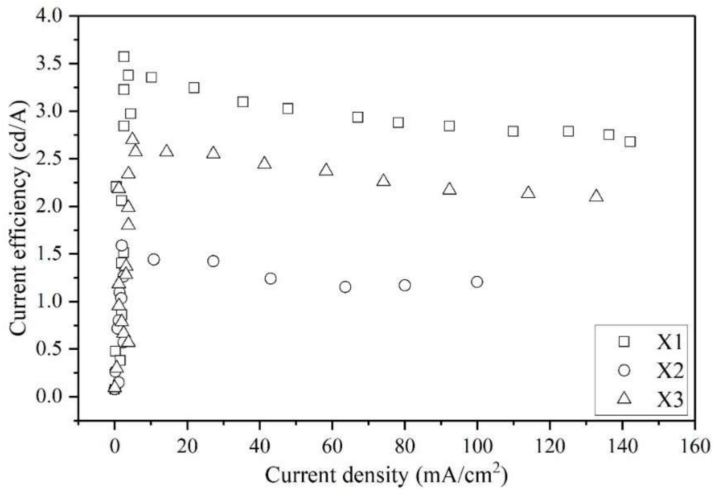

Fig. 10. The luminous efficiency of different devices varies with current efficiency

5. Conclusion

The article constructs a numerical analytical model based on the charge transport and luminescence efficiency in OLED devices, and uses the drift-diffusion model to describe the charge transport process in OLED devices. The truncation error in the numerical solution of the differential equation model is analyzed through the Taylor series expansion formula, and the numerical stability is analyzed theoretically. Based on this, the alternating solution method based on the improved Euler method and the iterative solution method is proposed to realize the charge transport and luminous efficiency solution of OLED devices. The study designs flexible OLED devices based on the theory of differential equation model, and verifies the feasibility of the differential equation model optimized devices through photophysical properties as well as comparative experiments.

The highest absorption peaks of the UV-Vis absorption spectrum, PL spectrum and phosphorescence spectrum of PEDOT:PSS molecule in toluene solution are located at 430, 460 and 527 nm, respectively. The luminescence performance of the comparison device and the optimized device in this paper is similar in terms of voltage variation and normalized spectra, while the lifetime of the optimized device reaches 95 h, which is longer than that of the comparison device. The charge transfer efficiency of the optimized device is as high as 99.99% and it shows the best light extraction efficiency as well as current efficiency.

The differential equation model established in the study provides a powerful theoretical tool for the optimization of charge transport and luminescence efficiency of OLED devices. Meanwhile, the research results can be applied to the development of OLED materials, device structure design and process optimization to promote the further development of OLED technology.

References

[1] Song, J., Lee, H., Jeong, E. G., Choi, K. C., & Yoo, S. (2020). Organic light-emitting diodes: pushing toward the limits and beyond. Advanced Materials, 32(35), 1907539.

[2] Shi, Y., Tu, Y., Wang, L., Zhang, Y., Zhang, Y., & Wang, B. (2021). Spectral influence of the normal LCD, blue-shifted LCD, and OLED smartphone displays on visual fatigue: A comparative study. Displays, 69, 102066.

[3] Shin, H. J., Kim, Y. H., Kim, D. M., Yun, S. H., Bae, S. J., Kim, H. S., ... & Oh, C. H. (2023). A novel ultra large size organic light emitting diode display for premium televisions. Journal of the Society for Information Display, 31(5), 253-263.

[4] Lehrer, M., Kim Wang, I., & Behnam, M. (2024). Lopsided Schumpeterian competition and the superstar firm phenomenon in OLED flat-panel displays. Technology Analysis & Strategic Management, 36(8), 1943-1959.

[5] Kim, B., Son, K., Kim, M., & Na, H. (2024). Tandem OLED: The Solution for In-Vehicle Displays in the SDV-Based EV Era. IDinformation display, 19.

[6] Pode, R. (2020). Organic light emitting diode devices: An energy efficient solid state lighting for applications. Renewable and Sustainable Energy Reviews, 133, 110043.

[7] Murawski, C., & Gather, M. C. (2021). Emerging biomedical applications of organic light-emitting diodes. Advanced Optical Materials, 9(14), 2100269.

[8] Zhou, A., Wang, H., Zhang, Y., & Hu, C. (2022). Recent progress of flexible OLEDs for wearable devices. Fiber and Integrated Optics, 41(1-2), 1-25.

[9] Choi, S., Jo, W., Jeon, Y., Kwon, S., Kwon, J. H., Son, Y. H., ... & Choi, K. C. (2020). Multi-directionally wrinkle-able textile OLEDs for clothing-type displays. Npj flexible electronics, 4(1), 33.

[10] Sun, N., Jiang, C., Li, Q., Tan, D., Bi, S., & Song, J. (2020). Performance of OLED under mechanical strain: a review. Journal of Materials Science: Materials in Electronics, 31, 20688-20729.

[11] Hong, G., Gan, X., Leonhardt, C., Zhang, Z., Seibert, J., Busch, J. M., & Bräse, S. (2021). A brief history of OLEDs—emitter development and industry milestones. Advanced Materials, 33(9), 2005630.

[12] Chen, F., & Kuo, J. (2022). In-vehicle display technology. In Advanced Driver Assistance Systems and Autonomous Vehicles: From Fundamentals to Applications (pp. 339-419). Singapore: Springer Nature Singapore.

[13] Jia, H. (2018). Who will win the future of display technologies?. National Science Review, 5(3), 427-431.

[14] Yuan, W. Z., Bin, X., Chen, G., He, Z., Liu, J., Ma, H., ... & Zhang, Y. (2017). Achieving hybridized local and charge-transfer excited state and excellent OLED performance through facile doping. Advanced Optical Materials, 5(21), 1700466.

[15] Lee, J. H., Chen, C. H., Lin, B. Y., Shih, Y. C., Lin, K. F., Wang, L., ... & Lin, C. F. (2018). Effect of trapped electrons on the transient current density and luminance of organic light-emitting diode. Journal of Physics D: Applied Physics, 51(14), 144003.

[16] Zhao, X., Tang, X., Zhu, H., Ma, C., Wang, Y., Ye, S., ... & Xiong, Z. (2021). Room-temperature observation for reverse intersystem crossing in exciplex-based OLEDs with balanced charge injection. ACS Applied Electronic Materials, 3(7), 3034-3043.

[17] Al-Qrinawi, M. S., El-Agez, T. M., Abdel-Latif, M. S., & Taya, S. A. (2021). Capacitance-voltage measurements of hetero-layer OLEDs treated by an electric field and thermal annealing. Int. J. of Thin Film Science and Technology, 10, 217-226.

[18] Gao, M., Burn, P. L., & Pivrikas, A. (2019). Charge transport in an organic light emitting diode material measured using metal-insulator-semiconductor charge extraction by linearly increasing voltage with parameter variation. Journal of Applied Physics, 126(3).

[19] Negi, S., Mittal, P., & Kumar, B. (2018). Impact of different layers on performance of OLED. Microsystem Technologies, 24, 4981-4989.

[20] Li, C., Li, Z., Yan, X., Zhang, Y., Zhang, Z., & Wang, Y. (2017). Structurally simple non-doped sky-blue OLEDs with high luminance and efficiencies at low driving voltages. Journal of Materials Chemistry C, 5(8), 1973-1980.

[21] Ullbrich, S., Benduhn, J., Jia, X., Nikolis, V. C., Tvingstedt, K., Piersimoni, F., ... & Vandewal, K. (2019). Emissive and charge-generating donor–acceptor interfaces for organic optoelectronics with low voltage losses. Nature materials, 18(5), 459-464.

[22] Kwon, S. K., Lee, E. H., Kim, K. S., Choi, H. C., Park, M. J., Kim, S. K., ... & Kwon, J. H. (2017). Efficient micro-cavity top emission OLED with optimized Mg: Ag ratio cathode. Optics Express, 25(24), 29906-29915.

[23] Lee, H., Cho, H., Byun, C. W., Han, J. H., Kwon, B. H., Choi, S., ... & Cho, N. S. (2018). Color-tunable organic light-emitting diodes with vertically stacked blue, green, and red colors for lighting and display applications. Optics express, 26(14), 18351-18361.

[24] Bauri, J., Choudhary, R. B., & Mandal, G. (2021). Recent advances in efficient emissive materials-based OLED applications: a review. Journal of Materials Science, 56(34), 18837-18866.

[25] Fadavieslam, M. R. (2019). The effect of thickness of light emitting layer on physical properties of OLED devices. Optik, 182, 452-457.

[26] Sangwook Park,Changmin Lee,Hyukmin Kwon,Saeyoung Oh,Kiho Lee,Seokwoo Kang... & Jongwook Park. (2025). High-efficiency blue OLED host materials based on new anthracene-dibenzofuran derivatives. Journal of Luminescence121106-121106.

[27] Kwesi Acheampong & Huiqing Zhu. (2025). Localized Hermite method of approximate particular solutions for solving the Poisson equation. Applied Mathematics Letters109471-109471.

[28] Xiao Zhong,Jiyuan Li,Letong Wang,Jie Chen,Xinxin Gong,Lin Xu... & Yunlong Yue. (2025). Cognitive and neural basis of vigilance advantage in soccer players: evidence from the drift-diffusion model and magnetic resonance imaging .Psychology of sport and exercise102804.

[29] Zulkifli Nur Shahirah,Samsudin Nooraida & Yusof N M M. (2022). Improving Euler Method using Centroidal-Polygon Scheme for Better Accuracy in Resistor-Capacitor Circuit Equation. Journal of Physics: Conference Series(1).

[30] Shuai Mo,Wenhao Song,Yingxin Zhang,Yuansheng Zhou,Bowei Yao,Haruo Houjoh & Wei Zhang. (2025). A new iterative method for calculating the time-varying meshing stiffness of orthogonal face gear pairs. Mechanism and Machine Theory105938-105938.